Design and Analysis of a Permanent Magnet Spherical Actuator*

Liang Yan, I-Ming Chen, Chee Kian Lim
School of Mechanical and Aerospace Engineering
Nanyang Technological University
Singapore 639798
michen@ntu.edu.sg

Guilin Yang, Wei Lin
Mechatronics Group
Singapore Institute of Manufacturing Technology
Singapore 638075
glyang@SIMTech.a-star.edu.sg

Kok-Meng Lee
George W. Woodruff School of Mechanical Engineering
Georgia Institute of Technology
Atlanta, Georgia, USA 30332-0405
kokmeng.lee@me.gatech.edu

***Abstract*— This paper has proposed a design concept of a spherical actuator including a ball-shaped rotor with a full circle of permanent-magnet (PM) poles and a spherical-shell-like stator with two layers of circumferential air-core coils. One key feature of this design is parametrization of the PM pole, which benefits the design optimization of the spherical actuator greatly. According to the magnetic field model, the variation of flux density with respect to PM-pole parameters can be revealed. Therefore, these parameters can be appropriately chosen to achieve a high magnetic flux density. Another advantage of this design is the singularity-free, which is verified within the workspace with torque model and condition numbers.**

***Index Terms*— Spherical actuator, Magnetic field model, Design optimization**

I. INTRODUCTION

The rapid advances in robotics and automatic manufacturing have brought about the demand of multi-degree-of-freedom (DOF) actuators to replace the conventional spherical motion mechanisms which are composed of several single-axis actuators. One of the effective options is the spherical actuator which can achieve a 2/3-DOF rotational motion in only one joint. This type of actuators have the virtues of compactness, uniform motion and nonsingularity etc. Williams and Laithwaite *et al*. have done some pioneer work on the spherical induction motor [1] [2]. Its magnetic field and torque were analyzed by Davey *et al* [3]. This induction motion can only achieve 2-DOF spherical motion. As an improvement, a 3-DOF induction spherical motor was conceptualized by Vachtsevanos *et al* [4]. However, owing to the complexity in mechanical and winding design, it is difficult to produce prototype. Lee *et al*. [5] have developed a variable-reluctance spherical motor, which has a compact size as well as a desirable working range. A nonlinear toque model relates the current inputs and the torque output, which is not favored by real-time control [6]. PM spherical actuators which can achieve either 2-DOF motion or 3-DOF motion are developed by Wang *et al* [7] [8]. The rotor completely consists of magnetized rare earth materials (NdFeB), i.e. the rotor pole's dimension has been fixed. This configuration increases not only the inertia moment of the rotor due to the high density of rare earth material (7.5g/mm^3) but also the system cost.

Generally speaking, electromagnetic motors offer advantages such as fast response, high torque and moderate voltage operation, etc. In addition, as an optional force/torque generating element of electromagnetic motors, PM has the virtue of no excitation losses because there is no electrical energy absorbed by the field excitation system [9]. For these reasons, a PM spherical actuator based on the electromagnetic principle [10] [11] is proposed in this research. More importantly, the rotor pole is parameterized, which contributes to the design optimization of this actuator. In our previous study [12], based on the parameterized poles, the magnetic field model and the torque model have been derived. The objective of this paper is to determine appropriate values of these parameters according to the theoretical models and analyze the nonsingularity of this spherical actuator.

In following sections, the working principle of this spherical actuator is introduced and the models of both the magnetic field and the torque are reviewed. According to the magnetic field model, the design optimization of PM & coil poles is considered. Based on the design optimization, a research prototype has been developed. After that, by taking advantage of the torque model, nonsingularity property of this spherical actuator design is verified.

II. WORKING PRINCIPLE & THEORETICAL MODELS OF THE PM SPHERICAL ACTUATOR

A. Working Principle

The working principle of this spherical actuator is illustrated in Fig. 1. This spherical actuator consists of a ball-shaped rotor with a full circle of PM poles and a spherical-shell-like stator with two layers of circumferential air-core coils. The rare earth PMs can generate high flux density within the actuator, and the air-core coils may simplify the torque model in a linear fashion. With a pair of coils activated in two longitudinal directions, the rotor creates tilting motions in two orthogonal directions as shown in Fig. 1(a) and (b). By energizing the rest of the circumferential coils, the rotor can spin about its axis. Therefore, through varying the input currents of the coils, the actuator can produce any desirable 3-DOF rotational motion within the workspace.

*This work is a collaborative research project among Nanyang Technological University, Singapore Institute of Manufacturing Technology and Georgia Institute of Technology under the project grant U02-A-040B.

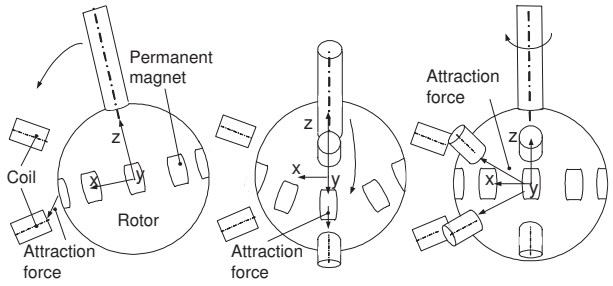

(a) First tilting motion (b) Second tilting motion (c) Spinning motion

Fig. 1. 3-DOF motion of spherical actuator

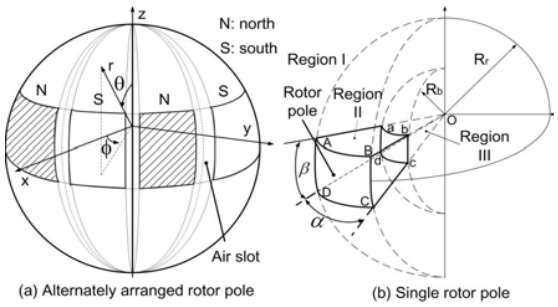

Fig. 2. Arrangement of the rotor poles

B. Magnetic Field Model

Figure 2(a) illustrates the alternately magnetized PM poles along the equator of the rotor. Note that air slots exist in between PM poles, which generalizes the study of poles pattern. Figure 2(b) shows the structure of a single PM pole clearly, i.e. the approximate dihedral cone enclosed by $ABCD$ and $abcd$. The dihedral cone can be defined by four parameters: latitudinal angle α, longitudinal angle β, rotor radius R_r and rotor core radius R_b. (The core can be used for the assembly of the spherical bearing.) The rotor space under study is divided into three regions. The air space outside the rotor is called Region I. The volume enclosed by $ABCD$ and $abcd$, the PM pole (filled with rare earth material), is called Region II. The inner core enveloped by $abcdO$ filled with ferromagnetic materials such as soft iron is called Region III. Only the radial component of the flux density is able to generate a torque with respect to the rotor center [12]. By using the Laplace's equation and the boundary conditions among these three regions, this radial component is formulated as

$$B_{Ir} = \frac{15\mu_0 M_0 c d_4}{8\pi}\sqrt{\frac{35}{2}} r^{-6}\sin^4\theta(a\cos 4\phi - b\sin 4\phi), \quad (1)$$

where μ_0 is the permeability of free space with the value of $4\pi \times 10^{-7}$H/m; θ, ϕ and r form the spherical coordinates affixed on the rotor frame as shown in Fig. 2(a); M_0 is the magnitude of the residual magnetization vector $\mathbf{M}_0$ (A/m) which is related to the remanence $\mathbf{B}_{rem}$ (T) by $\mathbf{M}_0 = \mathbf{B}_{rem}/\mu_0$; and

$$\begin{aligned} d_4 &= d_4^{\perp}/d_4^{\top}, \quad (2)\\ d_4^{\perp} &= R_r^6 + \frac{9\mu_{IIrc}R_b^6 R_r^9}{4(\mu_{IIIr}-\mu_{IIrc})R_b^9 - (4\mu_{IIIr}+5\mu_{IIrc})R_r^9},\\ d_4^{\top} &= 5(\mu_{IIrc}-1) + \\ &\quad \frac{9\mu_{IIrc}(4\mu_{IIIr}+5\mu_{IIrc})R_r^9}{4(\mu_{IIIr}-\mu_{IIrc})R_b^9 - (4\mu_{IIIr}+5\mu_{IIrc})R_r^9}, \end{aligned}$$

R_r (mm) is the rotor radius; R_b (mm) is the radius of Region III; the dimensionless quantity, μ_{IIrc} is the relative recoil permeability of the rare-earth material; μ_{IIIr} is the relative permeability of Region III; a, b and c can be calculated by following integral functions

$$\begin{aligned} a+bi &= \int_0^{2\pi}(-1)^{(p-1)}\cos(\phi - \frac{\alpha}{2} - \frac{\pi}{4}(p-1))e^{-im\phi}d\phi, \quad (3)\\ &\quad p = 1,2,3,...,8,\\ c &= \int_0^{\pi}\sqrt{\frac{2n+1}{4\pi}\frac{(n-m)!}{(n+m)!}}P_n^m(\cos\theta)\sin^2\theta d\theta, \quad (4) \end{aligned}$$

$P_n^m(\cos\theta)$ are associated Legendre functions [13]. To simplify the computation, only the fundamental terms, i.e. $n = 4$ and $m = \pm 4$ are considered in the derivation of the magnetic field. Note that these integrals are only valid within the range of

$$\begin{aligned} \frac{\pi}{4}(p-1) < &\quad \phi \quad < \frac{\pi}{4}(p-1) + \alpha, \quad p = 1,2,...8,\\ \frac{\pi}{2} - \frac{\beta}{2} < &\quad \theta \quad < \frac{\pi}{2} + \frac{\beta}{2}. \end{aligned}$$

For the rest non-magnetized regions in the rotor, the integral functions are equal to zero.

C. Torque Model

To develop a servo system for the position and speed control of the spherical actuator, torque modeling of the actuator is necessary. According to the $Lorentz$ force law [14], the orientation-dependant torque model of this spherical actuator that relates the torque output to the current input is derived [12]. The torque occurring between the i^{th} coil and the magnetic field of the rotor is

$$\mathbf{T}_i = \begin{bmatrix} T_{xi} \\ T_{yi} \\ T_{zi} \end{bmatrix} = T_c \begin{bmatrix} f_x(\theta_i,\phi_i) \\ f_y(\theta_i,\phi_i) \\ f_z(\theta_i,\phi_i) \end{bmatrix} J_i = T_c \mathbf{f}(\theta_i,\phi_i) J_i, \quad (5)$$

where

$$T_c = \sqrt{\frac{35}{2}}\frac{15\mu_0 M_0 c d_4}{16\pi}(R_0^{-2} - R_1^{-2}),$$

R_0 (mm), R_1 (mm) are distances from the rotor center to the top and bottom surfaces of the coil respectively as shown in Fig. 3; J_i (A/mm^2) is the current density passing thought the i^{th} coil; $f_x(\theta_i,\phi_i)$, $f_y(\theta_i,\phi_i)$ and $f_z(\theta_i,\phi_i)$ are trigonometric functions related to the orientation of the coil axis in the rotor frame which is specified by θ_i and ϕ_i. Consider the spherical actuator with a full set of coils. N torque equations similar

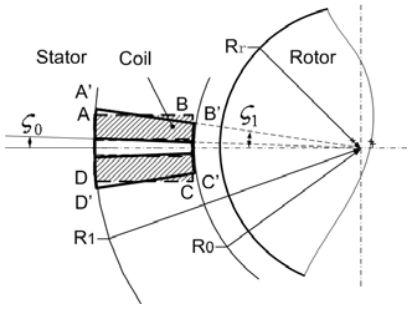

Fig. 3. Torque formulation (sectional view)

to Eqn. (5) can be obtained. Merging these torque equations into a matrix form yields

$$\mathbf{T} = T_c \begin{bmatrix} f_x(\theta_1,\phi_1)\, f_x(\theta_2,\phi_2) \cdots f_x(\theta_N,\phi_N) \\ f_y(\theta_1,\phi_1)\, f_y(\theta_2,\phi_2) \cdots f_y(\theta_N,\phi_N) \\ f_z(\theta_1,\phi_1)\, f_z(\theta_2,\phi_2) \cdots f_z(\theta_N,\phi_N) \end{bmatrix} \begin{bmatrix} J_1 \\ J_2 \\ \vdots \\ J_N \end{bmatrix}, \quad (6)$$

where $\begin{bmatrix} J_1 & J_2 & \cdots & J_N \end{bmatrix}^T$ is a vector of the currents passing through Coil 1, Coil 2, $\cdots$, Coil N. For brevity, let Q be the torque matrix, Eqn. (6) is then

$$\mathbf{T} = T_c Q \begin{bmatrix} J_1 & J_2 & \cdots & J_N \end{bmatrix}^T. \quad (7)$$

III. DESIGN OF PM & COIL POLES

High flux density in Region I contributes to high torque of the spherical actuator. Therefore, the purpose of the PM pole design is to achieve high flux density based on the magnetic field model. On the other hand, excessive mass of PM poles which does not increase the flux density evidently should be avoided. Design of the coil pole aims at more turns of wires to achieve a high torque.

A. Determination of α

Inspection of Eqn. (1) shows that the magnetic flux density is affected by the constants a, b and c, which in turn are determined by α and β according to Eqns. (3) and (4). To facilitate the following investigation, Eqn. (1) can be reorganized as

$$B_{Ir} = \frac{15\mu_0 M_0 c d_4}{8\pi} \sqrt{\frac{35}{2}(a^2+b^2)}\, r^{-6} \sin^4\theta \cos(4\phi+\phi_0), \quad (8)$$

where ϕ_0 is determined by $\cos\phi_0 = \frac{a}{\sqrt{a^2+b^2}}$ and $\sin\phi_0 = \frac{b}{\sqrt{a^2+b^2}}$. According to Eqn. (8), α affects the magnitude of the flux density through the term of $\sqrt{a^2+b^2}$. This property gives a means to choose a suitable α so that a reasonable magnetic flux density can be obtained. Through computation, the curve relating $\sqrt{a^2+b^2}$ to α is presented in Fig. 4(a). It can be seen that although $\sqrt{a^2+b^2}$ increases continuously within the range of $0 < \alpha < 45°$, the augmentation is neglectable after $\alpha = 40°$. Therefore, $\alpha = 40°$ is determined for the PM poles. This value offers additional benefits. (1) The remaining $5°$ angle provides space to design a fixture in the rotor frame for holding PM poles. (2) The mass/moment of inertia of the rotor is reduced considerably.

Asides from the magnitude of the flux density, α can also be used to analyze the positions where the flux density arrives at a maximum value. According to Eqn. (8), the magnitude of B_{Ir} takes the maximum value, when $\sin\theta = 1$ and $\cos(4\phi+\phi_0) = \pm 1$, i.e. when $\theta = \pi/2$ and

$$\phi = \frac{k}{4}\pi - \frac{\phi_0}{4}, k = 0, 1, 2, ..., 7. \quad (9)$$

Clearly, the condition of $\theta = \pi/2$ indicates that the maximum flux density must be along the equator of the rotor. Subsequently, the attention is restricted to the condition of $\phi = k\pi/4 - \phi_0/4$. The discussion begins with the special case of $k = 0$. It can be verified that a is a positive value whereas b is a negative one. In order to meet the requirement of $\cos\phi_0 = \frac{a}{\sqrt{a^2+b^2}} > 0$ and $\sin\phi_0 = \frac{b}{\sqrt{a^2+b^2}} < 0$, the phase of ϕ_0 has to be in the fourth quarter. In other words, $-\phi_0$ lies in the first quarter, or $0 < -\phi_0/4 < \pi/8$. Therefore, given a value of $a + bi$ that can be calculated from α according to Eqn. (3), the angle of $-\phi_0/4$ can be uniquely determined in the first quarter. In short, a mapping between α and ϕ_0 can be found. Because $\phi = -\phi_0/4$ is one position having maximum flux density, the mapping between α and $-\phi_0/4$ is considered. The relationship between $-\phi_0/4$ and α can be illustrated in Fig. 4(b). It is easy to find out that $-\phi_0/4$ is always half of α, i.e. $-\phi_0/4 = \alpha/2$. In physics, this result indicates that one of the maximum value of B_{Ir} ($k = 0$) is at the position of $\phi = \alpha/2$ or the center of PM-pole 1. Similarly, for $k = 1, 2, ..., 7$, the relation $\phi = k\pi/4 + \alpha/2$ holds. All these positions locate at the center lines of PM poles in ϕ direction. Consider both $\theta = \pi/2$ and $\phi = k\pi/4 + \alpha/2$. It can be seen that all of the maximum flux density are at the center points on top surfaces of eight PM poles.

B. Determination of β

According to Eqn. (4), the constant c is specified by the angle β of the PM pole through the integral range $\pi/2 - \beta/2 < \theta < \pi/2 + \beta/2$. From Eqn. (1), it can be seen that large c leads to high B_{Ir}. Hence, an appropriate value of β may result in high flux density B_{Ir}. As a matter of convenience, let $\beta_1 = \beta/2$, where β_1 varies from 0 to 90°. By using Eqn. (4), the relation between β_1 and the constant c is plotted in Fig. 5. Inspection shows that after the point of $\beta_1 = 35°$, c does not increase critically. Therefore, $\beta_1 = 35°$, i.e. $\beta = 70°$ is chosen for the design of PM pole.

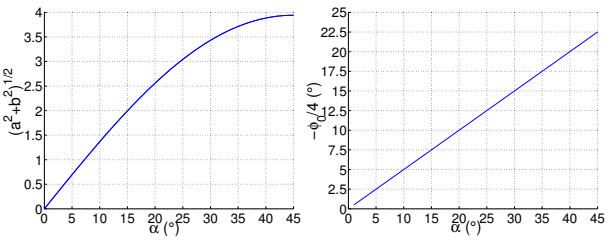

(a) Effect on magnitude (b) Position of maximum B_{Ir}

Fig. 4. Effect of α

C. Effect of R_r

According to Eqn. (1), the flux density is proportional to the constant d_4 which in turn is related to the R_r by Eqn. (2). In order to simplify the study, let $R_b = 0$. Figure 6(a) illustrates the relationship between R_r and d_4 explicitly. Approximately, the value of d_4 increases exponentially with respect to R_r. Therefore, large size of the rotor is theoretically preferred to create a high flux density. Obviously, huge size of the rotor is not feasible in practice. Due to the structural constraint in the spherical actuator, the rotor size is chosen as 46.5mm in our case.

D. Optimum Value of R_b

As long as parameters α, β and R_r are determined, the size of the PM pole is varied by R_b only as shown in Fig. 2. The larger is the value of R_b, the smaller is the size of PM pole. The relationship between R_b and $1/d_4$ reflected in Eqn. (2) can be plotted in Fig. 6(b). It can be seen that large size of PM pole, or small value of R_b produces higher magnetic flux density. However, when R_b shrinks to a certain value, such as 23mm indicated in Fig. 6(b), there is no evident increase of the flux density. This fact justifies the assumption of $R_b = 0$ when evaluating the effect of R_r in last subsection. As a result, $R_b = 23$mm is taken as the inner radius of the PM pole. This value allows a hollow space in the rotor core, which provides the assembling space for a spherical bearing as well as diminishes the inertia moment of the rotor.

Thus far, all dimensions of the PM pole have been determined, i.e. $\alpha = 40°$, $\beta = 70°$, $R_r = 46.5$mm and $R_b = 23$mm.

E. Coil Structure

The other critical element to generate a torque of the spherical actuator is air-core coils. The design of the coil is relatively straightforward. According to Lorentz force law, in order to achieve high torque which is favored by system performance, large number of winding turns are the purpose of coil design. Two types of coil structures have been proposed as shown in Fig. 7. Compared with the straight coil, the number of winding turns of the trapezoid-shaped coil can rise more than 50%. As a tradeoff, it is a challenge to wind and tauten the coil. Special fixtures and winding approach

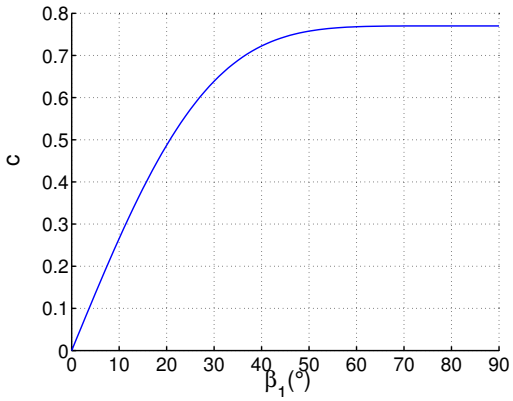

Fig. 5. Variation of constant c

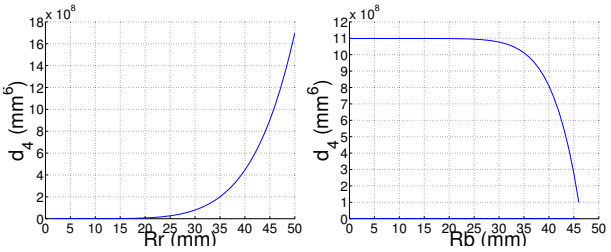

(a) Effect of R_r (b) Determination of R_b

Fig. 6. Effect of radial dimensions

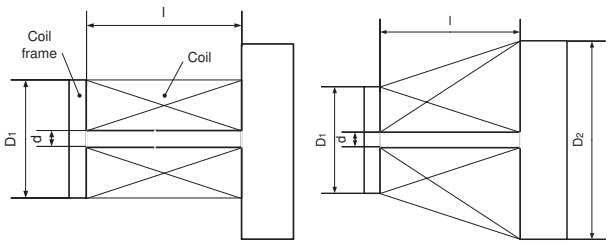

(a) Straight coil (b) Trapezoid coil

Fig. 7. Coil frames

for this type of coils are investigated in order to replace the current straight coil.

IV. NONSINGULARITY OF THE WORKSPACE

Singularities here are defined as certain orientations of the rotor where no motion or no torque can be generated with respect to the rotor center even though large currents are supplied. These singularities have to be strictly avoided in the design because they may cause severe malfunctions. In a mathematical sense, nonsingularity can be stated as for any $\mathbf{T}$ in Eqn. (6), there is at least one solution of $[J_1 J_2 ... J_N]^T$, which implies that the matrix Q in Eqn. (7) must have a full rank. Having known that the matrix Q is specified by the orientation angles of coils in the rotor frame, θ_i and ϕ_i, Q can also be determined by the rotor orientation in the stator frame. In other words, corresponding to each rotor orientation in the stator frame, a series of θ_i, ϕ_i and thus the matrix Q can be uniquely determined. Consequently, evaluating the nonsingularity attribute for every orientation of the rotor in the workspace suffices to justify the nonsingularity of this spherical actuator.

A straightforward way to verify the nonsingularity is to compute the rank of Q for every possible set of θ_i, ϕ_i, where $i = 1, 2, 3, ..., N$. If all ranks are equal to 3, i.e. Q is always a full rank matrix, the spherical actuator is totally singularity-free. Otherwise, singularities exist within the workspace. Although the straightforward way is clear and simple, it does not reveal how close the system includes singularity points. Therefore, another method based on the condition number of Q is proposed to satisfy this requirement.

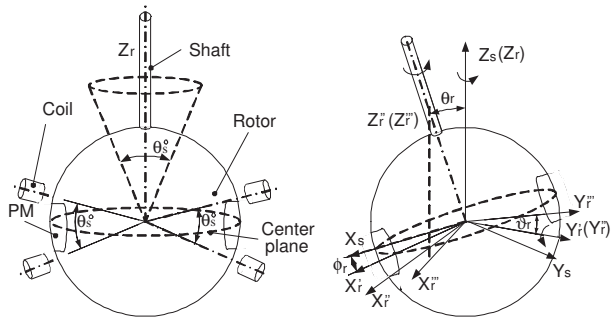

(a) Working range of rotor (b) Rotation of rotor

Fig. 8. Representation of the rotor orientation

A. Mathematical Background

Before verifying the nonsingulariy property of the spherical actuator, fundamental concept pertaining to the condition number [15] is briefly reviewed. The condition number for square/non-square matrices is computed from the characteristic roots or singular values of the matrix by

$$cond(Q) = \frac{\text{largest singular value}}{\text{smallest singular value}}.$$

Ideally, when $cond(Q) = 1$, the system possesses a good condition. When $cond(Q) \gg 1$, normally greater than 20, the system is ill-defined or nearly singular [16].

B. Representation of the Rotor Orientation

The workspace of the spherical actuator is shown in Fig. 8(a). Imagine that a series of PM poles are mounted along the equator of the rotor, whereas the coils on the stator point to the rotor center with the their axes. Additionally, the coils are symmetrically arranged with respect to the equatorial plane, with a angle θ_s between one pair of neighboring coils residing in different layers. It can be seen that the rotor can create a non-constrained spinning motion about its own z-axis, Z_r, wherever the rotor axis orients. However, when the rotor inclines to the position where one PM's axis is collinear with that of the coil, it cannot incline further in the same direction, i.e. the rotor reaches its boundary of the workspace. Based on this observation, it is conclude that Z_r axis of the rotor can only move within a cone-shaped workspace with a cone angle θ_s as shown in Fig. 8(a).

Next consider how an orientation of the rotor can be achieved. Let the initial orientation be the position where the rotor frame (X_r, Y_r, Z_r) coincides with the stator frame (X_s, Y_s, Z_s) (Fig. 8(b)). In order to arrive at an arbitrary final orientation within the workspace, three sequential rotations have to take place. (1) The rotor rotates about the Z_r axis by an angle of ϕ_r, ranging from 0° to 360°. (2) About the Y_r axis after the first rotation, the second rotation of θ_r occurs, ranging from 0 to $\theta_s/2$. This rotation along with the first one determine the direction of the rotor axis in the stator frame. (3) The spinning motion happens about the Z_r axis again by an angle of ϑ_r, ranging from 0 to 360°. Through these three rotations, any orientation of the rotor within the workspace can be achieved. Correspondingly, the three rotation matrices $R_z(\phi_r)$, $R_y(\theta_r)$ and $R_z(\vartheta_r)$ can be obtained [17].

C. Computation of Condition Number

1) Initial Values of θ_i and ϕ_i: Because the relative positions of coil's axes in the rotor frame at the starting orientation are known, it is easy to obtain the initial values of θ_i, ϕ_i, i.e. $\theta_{i0} = \pi/2 - \theta_s/2$, $\phi_{i0} = \pi/4(i-1)$ for Coil $i = 1, 2, ..., 12$, which form the top layer of the coils, and $\theta_{i0} = \pi/2 + \theta_s/2$, $\phi_{i0} = \pi/4(i-13)$ for Coil $i = 13, 14, ..., 24$, which compose the bottom layer of the coils. The subscript 0 represents the initial value of the i^{th} coil.

2) Unit Vector on the Coil Axis: Take a unit vector along the axis of the first coil. The coordinates of the end point of this vector in the rotor frame can be calculated as $\mathbf{p}_{10} = [\sin\theta_{10}\cos\phi_{10},\ \sin\theta_{10}\sin\phi_{10},\ \cos\theta_{10}]^T$.

3) Final Position of the Point: By using the three consequential rotations introduced previously, the final coordinates of the point $\mathbf{p}_{10}$ in the rotor frame can be obtained via following formula

$$\mathbf{p}_1 = [p_{1x},\ p_{1y},\ p_{1z}]^T = [R_z(\phi_r)R_y(\theta_r)R_z(\vartheta_r)]^T\mathbf{p}_{10}.$$

4) Computation of θ_1 and ϕ_1: According to the final position $\mathbf{p}_1$ relative to the rotor frame, θ_1 and ϕ_1 can be obtained in terms of p_{1x}, p_{1y} and p_{1z} as following

$$\theta_1 = \arccos\left(\frac{p_{1z}}{\sqrt{p_{1x}^2 + p_{1y}^2 + p_{1z}^2}}\right) = \arccos(p_{1z}), \quad (10)$$

$$\phi_1 = \begin{cases} \arccos\left(\dfrac{p_{1x}}{\sqrt{p_{1x}^2 + p_{1y}^2}}\right), & p_{1y} \geq 0, \\ -\arccos\left(\dfrac{p_{1x}}{\sqrt{p_{1x}^2 + p_{1y}^2}}\right), & p_{1y} < 0. \end{cases} \quad (11)$$

Note that because of the mechanical restrictions in the spherical actuator, $p_{1x}^2 + p_{1y}^2 \neq 0$.

5) Condition Number for One Orientation: Similarly, the steps of 2, 3 and 4 repeat for the remaining coils. Thus a complete set of θ_i and ϕ_i are obtained. Substituting all these values into Eqn. (6), the matrix Q can be eventually obtained. Subsequently, the condition number of Q corresponding to current rotor orientation is calculated.

6) Condition Numbers for all Orientations: Following the same process, calculation of the condition numbers is carried out for all attainable rotor orientations by varying ϕ_r, θ_r and ϑ_r in their respective ranges. If it turns out that all condition numbers are less than 20, then this spherical actuator is singularity-free. Otherwise, singularity points may exist in the workspace.

D. Visualization of the Result

Through computation of the condition number of Q within the workspace, it is found out that the minimum value of the condition number is 4.877, whereas the maximum value is 5.145. Both are far smaller than 20. Therefore this design of the spherical actuator is not only singularity-free but also far from the singularity positions.

The variation of the condition numbers can be presented visually for easy understanding. By fixing ϕ_r at certain

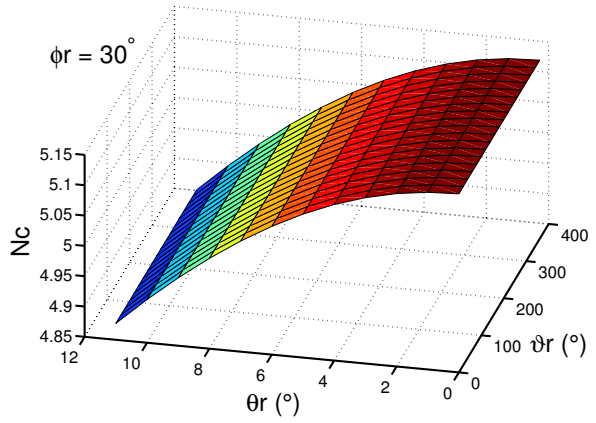

Fig. 9. Condition number ($\phi_r = 30°$)

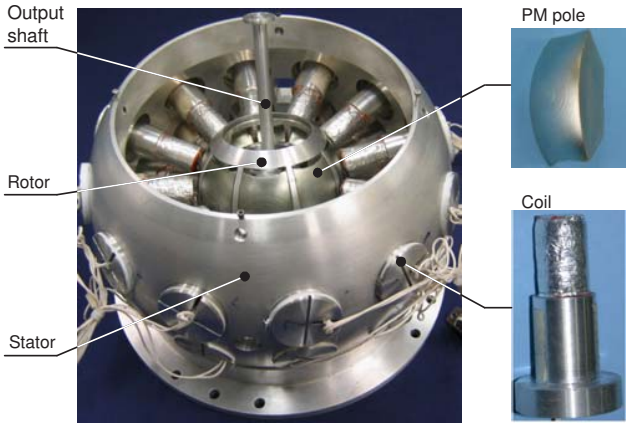

Fig. 10. Prototype of spherical actuator

values such as $0°, 15°, 30°, 45°$, etc, three variables, θ_r, ϑ_r and condition number, denoted as N_c, form a Cartesian coordinate. The variation of N_c is represented visually with a surface in this Cartesian coordinate. One example is shown in Fig. 9. Without loss of generality, only $\phi_r = 0° \sim 45°$ is considered due to the symmetric arrangement of the PM poles about the shaft.

V. Prototype Development

TABLE I
STRUCTURE SPECIFICATIONS OF SPHERICAL ACTUATOR

Inner / outer stator radius	95 / 112.5 (mm)
Rotor radius	46.5 (mm)
Number of rotor poles (PM)	8
Number of stator poles (coil)	24 / 2 layers
Maximum tilting angle	$\pm 11°$
Maximal torque	6 (Nm)

Based on the above analysis, a research prototype of the actuator has been developed as shown in Fig. 10. The specification is listed in Table I. The large size of stator is to facilitate the experimental research. For real product, the size can be reduced. This configuration allows more coils be incorporated into the stator so that the maximum tilting angle can be increased up to $\pm 45°$ and the resolution can also be improved. By using this prototype, experiments on magnetic field and torque variation can be carried out.

VI. Conclusion

The design concept of a PM spherical actuator with parameterized structure has been proposed. This parametrization offers the opportunity for design optimization. In addition, one effective method based on the condition number is taken to verify the singularity-free property of this design. Finally, according to the optimized dimensions, a prototype is developed for future experimental works.

Acknowledgment

The authors would like to acknowledge the assistance from Mr. Jialin Su, Dr. Weihai Chen and Mr. Thng Soong Moong Thomas.

References

[1] F. Williams, E. R. Laithwaite, and J. F. Eastham. Develpment and design of spherical induction motors. In *Proceeding of Institute of Electrical Engineers*, volume 106A, pages 471–484, December 1959.
[2] E. R. Laithwaite. Design of spherical motors. *Electrical Times (London)*, 9:921–925, June 1960.
[3] K. Davey, G. Vachtsevanos, and R. Powers. The analysis of fields and torques in spherical induction motors. *IEE Transactions on Magnetics*, 23(1):273–282, January 1987.
[4] G. J. Vachtevanos, K. Daveyand, and K. M. Lee. Development of a novel intelligent robotic manipulator. *IEEE Control Systems Magazine*, 7(3):9–15, June 1987.
[5] K. M. Lee, R. B. Roth, and Z. Zhou. Dynamic modeling and control of a ball-joint-like variable-reluctance spherical motor. *ASME Journal of Dynamic Systems, Measurement, and Control*, 118(1):29–40, March 1996.
[6] Z. Zhou. *Real-Time Control and Characterization of a Variable Reluctance Spherical Motor*. PhD thesis, Georgia Institute of Technology, GA, USA, May 1995.
[7] J. Wang, G. W. Jewell, and D. Howe. Spherical actuators with multiple degrees-of-freedom. In *IEE Colloquium on Limited motion electrical actuation systems*, number 1998/494, pages 8/1–8/6, October 1998.
[8] J. Wang, G. W. Jewell, and D. Howe. A novel spherical actuator with three degrees-of-freedom. In *IEEE Transactions of Magnetics*, volume 34, pages 2078–2080, June 1998.
[9] J. F. Gieras and M. Wing. *Permanent Magnet Motor Technology*. Marcel Dekker, Inc., 1998.
[10] C. K. Lim, L. Yan, I. M. Chen, G. L. Yang, and W. Lin. Mechanical design & numerical electromagnetic analysis of a dc spherical actuator. In *2004 IEEE Conference on Robotics, Automation and Mechatronics*, pages 536–541, Singapore, December 2004.
[11] L. Yan, C. K. Lim, I. M. Chen, G. L. Yang, and W. Lin. A hybrid approach for magnetic field analysis. In *2004 IEEE Conference on Robotics, Automation and Mechatronics*, pages 530–535, Singapore, December 2004.
[12] L. Yan, I.M. Chen, C.K. Lim, G.L. Yang, W. Lin, and K. M. Lee. Torque modeling of a spherical actuator based on lorentz force law. In *2005 IEEE International Conference on Robotics and Automation*, pages 3657–3662, Barcelona, Spain, April 2005.
[13] N. Virchenko and I. Fedotova. *Generalized Associated Legendre Functions and Their Applications*. World Scientific Publication, USA, 2001.
[14] N. O. M. Sadiku. *Elements of Electromagnetics*. Oxford University Press, USA, 2001.
[15] E. P. Gill, W. Murray, and H. M. Wright. Numerical linear algebra and optimization, 1991.
[16] http://economics.about.com/library/glossary/bldef-condition number.htm. Condition number.
[17] J. J. Craig. *Introduction to Robotics: Mechanics and Control*. Addison-Wesley Publishing Company, USA, 1989.